Spectral signatures of the diffusional anomaly in water

Anirban Mudi and Charusita Chakravarty[a)]
Department of Chemistry, Indian Institute of Technology—Delhi, New Delhi 110016, India

Ramakrishna Ramaswamy
School of Physical Sciences, Jawaharlal Nehru University, New Delhi 110067, India

(Received 28 September 2004; accepted 29 December 2004; published online 11 March 2005)

Power spectra for various tagged particle quantities in bulk extended simple point charge model water [H. J. C. Berendsen, J. R. Grigera, and T. P. Straatsma, J. Phys. Chem. **91**, 6269 (1987)] are shown to have a regime with $1/f^{\alpha}$ dependence on frequency f with α lying between 1 and 1.5 if the dynamical changes in the particular observable are sensitive to the multiple time-scale behavior of the hydrogen-bond network. The variations in mobility associated with the diffusional anomaly are mirrored in the scaling exponent α associated with this multiple time-scale behavior, suggesting that monitoring of $1/f^{\alpha}$ behavior is a simple and direct method for linking phenomena on three distinctive length and time scales: the local molecular environment, hydrogen-bond network reorganizations, and the diffusivity. Our results indicate that experimental studies of supercooled water to probe the density dependence of $1/f^{\alpha}$ spectral features, or equivalent stretched exponential behavior in time-correlation functions, will be of interest. © *2005 American Institute of Physics*. [DOI: 10.1063/1.1860555]

I. INTRODUCTION

Water displays a number of thermodynamic and kinetic anomalies when compared to simple liquids, particularly at low temperatures and pressures.[1–7] For example, the density anomaly is associated with a region in the temperature-density plane within which the thermal expansion coefficient is negative. Similarly, a region of anomalous diffusivity can be defined for which molecular mobility increases with compression. Along an isotherm, this anomalous diffusional regime is bounded by densities corresponding to the diffusivity minimum and maximum. In a qualitative sense, it is obvious that these anomalous features of water must be related to the special structural features of water: a strong preference for local tetrahedral order and the presence of a fluctuating three-dimensional network of hydrogen, bonds. Recently, using computer simulations, it has become possible to make more quantitative connections between structural features, the underlying potential energy landscape and macroscopic properties.[8–17]

Each water molecule can form at most four hydrogen bonds resulting in an open, tetrahedral network structure in the bulk. The strength of hydrogen bonds is estimated to lie between $5k_BT$ and $10k_BT$ at melting.[18] While this is strong enough that a substantial fraction of hydrogen bonds will be intact at room temperature, thermal fluctuations will be large enough to ensure that such bonds will have a finite lifetime of the order of picoseconds. As a result, the dynamics of the liquid, specially in the supercooled states, will be dominated by the behavior of the three-dimensional, hydrogen-bonded network, parts of which are constantly broken and reformed.

In this work, we focus on the relationship between the diffusional anomaly and the dynamics of this hydrogen-bonded network. Networks are typically characterized by multiple time scales due to the coupling of a large number of sites. Multiple time scale behavior is known to give rise to a stretched exponential behavior in the time-correlation functions $C(t)$ with $C(t)=C(0)\exp[-(t/\tau)^{\beta}]$ and a $1/f^{\alpha}$ type dependence on the frequency f with α close to 1 in the corresponding power spectrum, $S(f)$.[19–22] In analyzing power spectra, a value of α between 0.5 and 1.5 is taken to be a signature of long-range dynamical correlations and is frequently referred to as $1/f$ noise. White noise corresponds to $\alpha=0$. An α value of 2 is expected in the case of Brownian noise or in the presence of single, rather than multiple, time scales. The extent, the exponent and the frequency range of $1/f^{\alpha}$ noise can be used to as *quantitative* measures to characterize network dynamics. In the case of water, the individual sites can be identified as single water molecules with the network connectivity being determined by the magnitude of hydrogen-bond energies relative to the strength of thermal fluctuations. The rotational and translational modes of individual molecules are strongly modified by the tetrahedral network and are better described as librations and intermolecular vibrations. The intermolecular vibrational frequencies can be thought of as cooperative rearrangements on different size and time scales which scale with the number of molecules involved. Thus the hydrogen-bonded network will have a multiplicity of time scales, starting with the high frequency librational modes and followed by two-molecule O–O stretches, three-molecule O–O–O bends, etc.

In a set of molecular dynamics studies of water, we have used power spectral analysis to study dynamical correlations in observables sensitive to the local molecular environment that are likely to be strongly affected by network formation due to hydrogen bonding.[23–27] The observables examined in-

[a)]Author to whom correspondence should be addressed; FAX: (+) 91 112686 2122; Electronic mail: charus@chemistry.iitd.ernet.in

cluded tagged particle potential and kinetic energies, local tetrahedral order parameters and coordination numbers. The power spectrum was defined as

$$S(f) = \left| \int_{t_{\min}}^{t_{\max}} (A(t) - \langle A \rangle) e^{2\pi i f t} dt \right|^2, \quad (1)$$

where $A(t)$ is a time-dependent mechanical quantity with trajectory average $\langle A \rangle$. If the underlying dynamical processes span a frequency range from λ_1 to λ_2, the power spectrum will show a $1/f$ regime ($\alpha \approx 1$) for $\lambda_1 < f < \lambda_2$, a white noise regime for $f \ll \lambda_1 (\alpha = 0)$ and a Lorentzian tail ($\alpha \approx 2$) for $f \gg \lambda_2$.[22] A separation of two decades in time scales between λ_1 and λ_2 is adequate for observing a $1/f^\alpha$ regime with α close to 1. Unless otherwise stated, in this work, reference to $1/f^\alpha$ behavior will imply the multiple time-scale regime with α close to 1, rather than the Lorentzian tail with $a \approx 2$. It should also be noted that wherever there may be some confusion, we have used α' to denote the exponent of the Lorentzian tail and α for the multiple time-scale regime. The range of $1/f^\alpha$ behavior depends on both the observable and the temperature. The $1/f^\alpha$ behavior was most pronounced for the tagged particle potential energy and, at 300 K, the $1/f^\alpha$ regime stretched from 1 to 200 cm^{-1}. The exponent associated with the multiple time-scale regime was shown to be strongly correlated with the diffusivity, specially at temperatures of 300 K or less. The spectral features of the $1/f^\alpha$ regime could be related with the structure of the underlying static distributions of the tagged particle quantities.

We study the variation in the scaling exponent in the $1/f^\alpha$ regime to probe the multiple time-scale behavior of the hydrogen-bonded network as a function of both density and temperature. The SPC/E model for water is known to display the key thermodynamic and kinetic anomalies of water and is used in the molecular dynamics simulations. The computational details are summarized in Sec. II of this paper. Our results are presented in Sec. III. The scaling exponent of the $1/f^\alpha$ regime closely mimics variations in the diffusivity with density. Indeed, the boundaries of the region of the diffusional anomaly in the density-temperature plane can be constructed merely by examining the $1/f^\alpha$ exponent. Thus a long-time averaged transport property, such as the diffusivity, can be connected with the temporal fluctuations associated with the local order or local configurational energy on time scales of picoseconds. Monitoring of $1/f^\alpha$ behavior is therefore a simple and direct method for linking phenomena on three distinctive length and time scales: the local molecular environment, hydrogen-bond network reorganizations and the diffusivity. Key conclusions and implications for other networked and hydrogen-bonded liquids are summarized in Sec. IV.

II. COMPUTATIONAL DETAILS

A. The SPC/E model

The SPC/E model for water assumes that the water molecule can be treated as a rigid, nonpolarizable entity.[28] Each water molecule carries three charged sites which are located at the atomic positions and are associated with the corresponding atomic masses. The OH distance is 1.0 Å and HOH angle is equal to 109.47°, with partial charges on oxygen and hydrogen of $-0.8476e$ and $+0.4238e$, respectively. The Lennard-Jones site is located at the oxygen atom and the corresponding parameters are $\sigma = 3.166$ Å and $\epsilon = 0.6517$ kJ/mol. The configurational potential energy of the system is calculated by assuming pairwise additive interactions between water molecules.

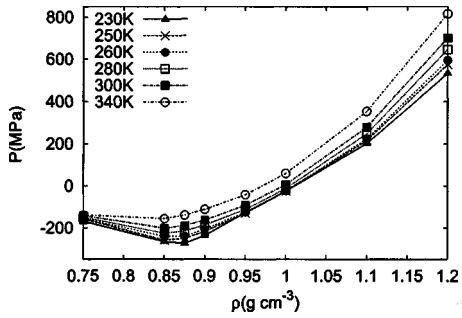

FIG. 1. Pressure P as a function of density ρ for SPC/E water along different isotherms. Systems at a density of 0.75 g cm^{-3} are likely to be inhomogeneous.

B. Molecular dynamics

The molecular dynamics simulations were performed using the DL_POLY software package.[29,30] *N-V-T* ensemble simulations for 256 SPC/E water molecules contained in a cubic simulation cell were carried out using the SHAKE algorithm with a timestep of 1 fs. Electrostatic interactions were evaluated using Ewald summation.[31] A Berendsen thermostat was used to maintain the desired temperature. An appropriate value for the thermostat time constant τ_B was made after studying its effect on various dynamical quantities.[25] Our simulation results are in reasonable agreement reported in Refs. 11 and 15, given the different techniques for evaluating long-range forces (Ewald as opposed to reaction field) and the statistical error bars. Simulations were carried out at six temperatures (230, 250, 260, 280, 300, and 340 K) along ten isochores (0.75, 0.85, 0.875, 0.9, 0.95, 1.0, 1.1, 1.2, 1.3, and 1.4 g cm^{-3}). At each state point, the system was equilibriated for a time period of 2–5 ns. Production run lengths were kept at 2 ns with $\tau_B = 200$ ps. Additional runs were carried out at three temperatures (280, 300, and 340 K) with production run lengths of 8.4 ns and $\tau_B = 1000$ ps as a check on the results.

Figure 1 shows the $P(\rho)$ curves at different temperatures which may be compared with the results give in Ref. 13. It can be seen that for all densities below 1 g cm^{-3}, the pressures are negative for the temperatures studied, indicating that water is stretched rather than compressed. The isothermal compressibility, defined as $\kappa_T = (1/\rho)(\partial P/\partial \rho)$, is negative only for the $\rho = 0.75$ g cm^{-3} isochore. The spindonal density for which $\kappa_T = 0$ is located between 0.85 and 0.875 g cm^{-3}. Below this density, the system is likely to be inhomogeneous. In our simulations, the state points along the 0.75 g cm^{-3} isochore are thermodynamically unstable; however, for consistency with previous simulation work on the diffusional anomaly we consider this density.

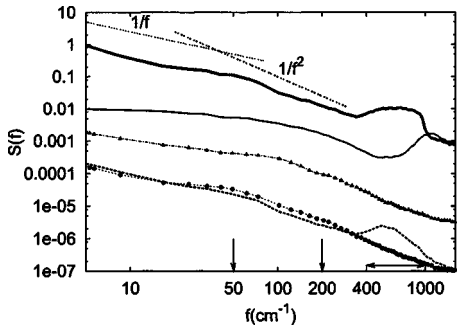

FIG. 2. Power spectra associated with temporal fluctuations in different tagged particle quantities at 230 K and 0.9 g cm^{-3}. The different curves represent $S_u(f)$ (thick solid line), $S_{\mathrm{lib}}(f)$ (solid line), $S_{\mathrm{NN}}(f)$ (filled triangles), $S_{\mathrm{O}}(f)$ (filled circles), and $S_{\mathrm{H}}(f)$ (dashed line). Arrows show the O–O stretch (200 cm^{-1}), O–O–O bend (50 cm^{-1}), and the librational region (400–1000 cm^{-1}) (Ref. 33).

C. Generating power spectra

Tagged particle quantities for 64 molecules were stored at intervals of 10 fs from the 2 ns production runs. This sampling interval corresponds to a Nyquist frequency of 1666 cm^{-1}. The values of τ_B provide the lower limit on the frequency range over which we can obtain reliable power spectra; thus, $\tau_B = 200$ ps corresponds to a lower frequency limit of 0.165 cm^{-1}. Standard fast Fourier transform routines were used with a square sampling window.[32] The normalization convention was chosen such that the integrated area under the $S(f)$ curve equaled the mean square amplitude of the time signal. Windows containing 2^{15} data points were used for Fourier transformation. Statistical noise in the power spectra was reduced by averaging over overlapping time signal windows as well as over individual tagged particle spectra. In a given frequency interval showing $1/f^{\alpha}$ behavior, linear least squares fitting of $\ln S(f)$ was done to obtain the α values. Variations in α values calculated from three independent simulations for the densities 0.9, 1.1, and 1.4 g cm^{-3} at 230 K were found to be less than 2%.

III. RESULTS AND DISCUSSION

A. Characteristics of power spectra associated with different observables

A number of different properties of tagged molecules were studied by us in an effort to determine which observables were most sensitive to the multiple time-scale behavior of the hydrogen-bonded network. Each of the observables shows somewhat different power spectral characteristics, as illustrated in Fig. 2 which shows the power spectra associated with different tagged particle quantities for bulk SPC/E water at 230 K and 0.9 g cm^{-3}.

1. Tagged molecule potential energy

The tagged molecule potential energy $u(t)$ corresponds to the interaction energy of an individual molecule with all the other molecules in the system. Since the configurational potential energy is assumed to be pair additive, the total potential energy, $U(t) = 0.5\Sigma_i u_i(t)$ where the sum extends over all molecules. The corresponding power spectrum $S_u(f)$ shows a broad peak, centered around 500 cm^{-1}, due to the high-frequency, essentially single-molecule, librational modes. The $S_u(f)$ curve shows two regions of $1/f^{\alpha}$-type behavior: (i) the high frequency 60–298 cm^{-1} range with $\alpha_u' = 1.56 \pm 0.02$ and (ii) the low frequency 1–40 cm^{-1} region with $\alpha_u = 1.06 \pm 0.02$. The O–O stretch and O–O–O bending modes for bulk SPC/E water are known to occur at 200 and 50 cm^{-1}, respectively,[33] and therefore the high frequency $1/f^{\alpha'}$ regime involves two or three-molecule hydrogen-bond network rearrangements. Since increasing delocalization of vibrational modes results in lowering of the frequencies, the low frequency $1/f^{\alpha}$ regime must involve displacements of four to six molecules. Results presented in Ref. 26 show that crossover to Markovian or white noise behavior does not occur for frequencies as low as 0.1 cm^{-1}; however, with increasing temperature, the crossover to white noise occurs at higher frequencies. Thus, at this state point, the power spectral profile may be thought of as having a multiple time-scale region between 1 and 40 cm^{-1} which has a high-frequency Lorentzian tail beyond 60 cm^{-1} and a crossover to white noise behavior below 0.1 cm^{-1}. The librational peak is distinct from the Lorentzian tail.

2. Tagged molecule kinetic energies

The kinetic energy of an individual molecule can be thought of as a measure of the strength of local thermal fluctuations. It can be subdivided into center-of-mass and librational contributions, since the rigid monomer approximation implies that there are no intramolecular vibrational modes to account for. The power spectra of the tagged particle center-of-mass kinetic energy was found to be essentially a white noise spectrum with no evidence of multiple time-scale behavior for a temperature as low as 213 K and is therefore not considered here.[24] The librational kinetic energy is defined as the difference between the total and the center-of-mass kinetic energies of a rigid molecule. The corresponding power spectrum $S_{\mathrm{lib}}(f)$ shows just a single prominent peak due to the librational modes but no multiple time-scale region. Note that the peak in $S_{\mathrm{lib}}(f)$ occurs at twice the frequency seen in the $S_u(f)$ spectrum.

3. Local structural order

The local structural order around a tagged oxygen atom is gauged by two order parameters, q_{O} and q_{H}. The degree of tetrahedrality of the four nearest hydrogen atoms surrounding a given oxygen atom i is measured by

$$q_{\mathrm{H}} = 1 - \frac{3}{8}\sum_{j=1}^{3}\sum_{k=j+1}^{4}(\cos\psi_{jk} + 1/3)^2, \tag{2}$$

where ψ_{jk} is the angle between the bond vectors $\mathbf{r}_{ij}$ and $\mathbf{r}_{jk}$ where j and k label the four nearest hydrogen atoms. The q_{O} order parameter is similarly defined using the positions of the four nearest oxygen atoms.[8] As the hydrogen-bond network is destroyed, the q_{O} order parameter will go to zero; in contrast, the q_{H} parameter will reach a limiting nonzero value due to the two bonded hydrogen attached to each oxygen atom. The q_{O} order parameter, in conjunction with a translational order parameter, has been previously used to charac-

terize the region of the phase diagram within which anomalous diffusional and density dependence could be expected.[8,9]

The power spectra corresponding to fluctuations in q_O and q_H are labeled $S_O(f)$ and $S_H(f)$, respectively. The $S_H(f)$ curve shows a clear peak due to librational motion, unlike the $S_O(f)$ curve. Both $S_O(f)$ and $S_H(f)$ spectra show two $1/f^{\alpha}$ regimes with different exponents but in the case of $S_O(f)$, the higher frequency $1/f^{\alpha'}$ regime stretches up to 1000 cm^{-1}. As in the case of $S_u(f)$, one can think of the low frequency $1/f^{\alpha}$ and high frequency $1/f^{\alpha'}$ regions as the multiple time-scale regime and the Lorentzian tail, respectively.

4. Local coordination numbers

We have used two different measures for the local coordination number, the number of hydrogen bonds of a given molecule n_{HB}, and the number of nearest neighbors n_{NN}. Following Ref. 12, a hydrogen bond was assumed to exist between for an O–H–O triplet if the oxygen-oxygen distance was less than 3.2 A° and the oxygen-hydrogen distance was less than 2.5 A°. Two molecules were defined to be nearest neighbors if the corresponding oxygen atoms were within a cutoff distance of 3.2 A°. In the earlier study, it was shown that as density increased, n_{NN} increased much faster than n_{HB} resulting in the creation of defects in the tetrahedral network and allowing for the anomalous increase in diffusivity with temperature. Beyond the diffusivity maximum, the rise in n_{NN} was assumed to decrease diffusivity due to steric effects. We have calculated the power spectra associated with fluctuations in both n_{NN} and n_{HB} and found that the behavior essentially parallels that of $S_O(f)$; therefore Fig. 2 shows the power spectrum corresponding to only to fluctuations in n_{NN}.

To summarize, the key features of the power spectral profiles are (i) a broad librational peak (ii) a high-frequency $1/f^{\alpha'}$ regime above 50 cm^{-1} with exponent α', and (iii) a second, low-frequency multiple time-scale regime in the range 1–40 cm^{-1} with a different exponent α. The low-frequency region may be identified as the true multiple time-scale regime while the high-frequency region corresponds to the Lorentzian tail. A white noise region ($\alpha=0$), seen at very low frequencies, becomes more pronounced at higher temperatures and/or higher densities, as discussed below. The librational peak is seen in $S_u(f)$, $S_H(f)$ and $S_{lib}(f)$ while the multiple time-scale regions are seen in all power spectra except $S_{lib}(f)$. At this temperature and density, the librational peak is fairly well separated from the Lorentzian tail of the multiple time-scale regime. At a given state point, the exact values of the exponents in the $1/f^{\alpha}$ regimes as well as the crossover frequencies depend on the specific quantities studied. The power spectra in Fig. 2 are normalized to ensure that the area under the curve corresponds to the mean squared amplitude of the time correlation function. The fluctuations in the local potential energy can therefore be seen to be the strongest. In addition, the $S_u(f)$ spectrum shows all the key power spectral features outlined above, making it the most convenient quantity for looking at multiple time-scale features of the hydrogen-bonded network.

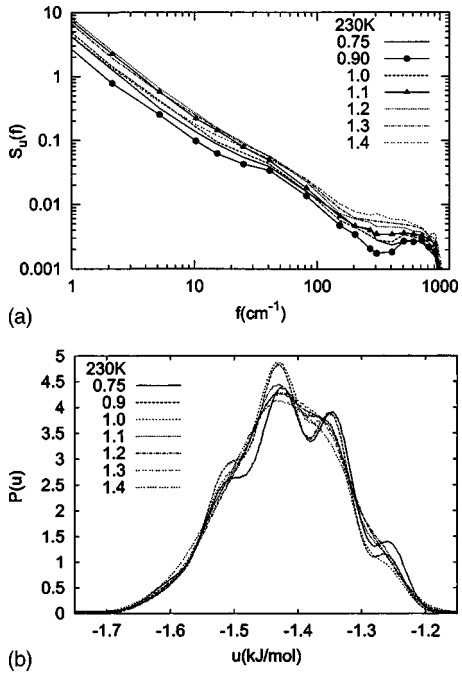

FIG. 3. (a) Power spectra $S_u(f)$ at different densities (in g cm^{-3}) along the 230 K isotherm. (b) Corresponding static distributions of tagged particle potential energies (in kJ mol^{-1}) at 230 K.

B. Density dependence of different features of the power spectrum

The existence of the diffusional anomaly in water suggests that the dynamics of the hydrogen-bonded network changes significantly with density which must be reflected in the power spectra. Figure 3(a) shows $S_u(f)$ at different densities for the 230 K isotherm. At this temperature, extended simple point charge model (SPC/E) water has a diffusional minimum and maximum at $\rho_{min}=0.9$ g cm^{-3} and $\rho_{max}=1.1$ g cm^{-3}, respectively.[12,14]

We first consider the qualitative changes in the librational region of the $S_u(f)$ curves with density along the 230 K isotherm. The librational peak is most clearly demarcated at $\rho_{min}=0.9$ g cm^{-3} indicating that decoupling of librational modes from the hydrogen-bonded network rearrangements is maximal at this density which is close to the density of crystalline ice. The librational peak moves to lower frequencies with increasing density and, for $\rho>\rho_{max}$, becomes a shoulder. Thus the frequency separation between the librational peak and the network rearrangements disappears with density. We thus provide direct dynamical evidence that the anomalous diffusional regime, for which $dD/d\rho>0$, is associated with increasing coupling of the librational modes with vibrations of the hydrogen-bonded network as density increases. This has been conjectured in earlier work based on static structural distributions.[12,16,17] The behavior of the librational peak in $S_{lib}(f)$ and $S_H(f)$ at 230 K is similar to that seen for $S_u(f)$. The increase in density at a given temperature clearly destroys hydrogen bonding and local tetrahedral order, facilitating coupling of librational modes with network vibrations.

We now consider the changes in the multiple time-scale region of the power spectrum as a function of density. The

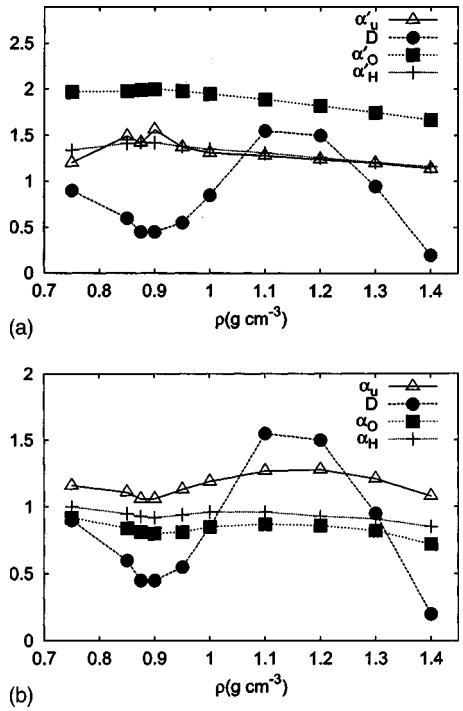

FIG. 4. Behavior of the exponent associated with the $1/f^{\alpha}$ regimes as a function of density at 230 K. Part (a) shows the exponents associated with the high-frequency $1/f^{\alpha}$ regime with α_u', α_H', and α_O' evaluated over the frequency ranges 60–298, 90–298, and 200–1000 cm^{-1}, respectively. Part (b) shows the exponents associated with the low-frequency $1/f^{\alpha}$ regime with α_u, α_H, and α_O evaluated over the 1–40 cm^{-1} range. Also shown is the diffusivity D in units of 2×10^{-6} cm^2/s.

major qualitative change is that the exponents of the multiple time-scale region and the Lorentzian tail become very similar with increasing density, suggesting that compression destroys the distinct identity of the Lorentzian tail. In our earlier work, the existence of the Lorentzian tail was correlated with a strongly multimodal distribution of underlying tagged particle energies, as shown in Fig. 3(b).[26]

The density-dependent changes in the exponents of the multiple time-scale and Lorentzian frequency regimes are shown in Fig. 4. At 230 K, the diffusivity D is correlated with the low-frequency (1–40 cm^{-1}) exponent α of the multiple time-scale region of $S_u(f)$, $S_O(f)$, and $S_H(f)$. The exponent α' of the Lorentzian tail (60–298 cm^{-1}) has a maximum at the density of minimum diffusivity. Beyond this density, α', values for $S_u(f)$, $S_O(f)$, and $S_H(f)$ power spectra decrease monotonically with density as compression results in attenuation of the Lorentzian tail.

We first consider the density-dependent changes in α_u' and α_u which vary most strongly with density. We note that at ρ_{min}, the librational modes will be most effectively decoupled from the network vibrations, the range of available frequencies contributing to the $1/f$ regime will be the narrowest and the Lorentzian tail will be most pronounced. This is consistent with our observation that α_u' is maximum and α_u is ≈1 at ρ_{min}. In physical terms, it implies that at 230 K and close to ρ_{min}, vibrational modes involving three or less molecules are significantly decoupled from more delocalized network reorganizations. As one moves away from ρ_{min}, α_u' decreases as the librational peak becomes progressively integrated into the vibrational band associated with the network rearrangements.

The correlation between the diffusivity and the exponent α_u of the multiple time-scale region of the power spectrum is very interesting because it links a zero frequency, equilibrium transport property with fluctuations in local properties of the network on time scales of picoseconds. The explanation for this correlation lies in the fact that diffusion in water can proceed by coupling of single-molecule librational modes to network vibrations. Essentially, librations result in weakening of hydrogen bonds and facilitate translational motion through the network. This rotational-translational coupling mechanism for diffusion cannot exist in simple liquids. Where diffusion proceeds essentially by means of thermal fluctuations or collisions. The relative importance of the two diffusional mechanisms will depend on temperature. At low temperatures, as librational modes become progressively more coupled to the network vibrations with increasing density, the diffusivity rises. In the context of power spectral analysis, this corresponds to the introduction of relatively localized, high frequency components into the multiple time-scale regime, resulting in an increase in α_u with density in the anomalous regime between ρ_{min} and ρ_{max}. The decrease in α_u with increasing density for $\rho>\rho_{max}$ is due to increasing importance of steric effects which force the system to behave more like a simple liquid with $\alpha=0$.[23]

The α_H and α_O values, characterizing the multiple time-scale region of $S_H(f)$ and $S_O(f)$, respectively, show density-dependent variations which are qualitatively similar to those seen for α_u. This is to be expected given that the hydrogen-bonding energy of an individual molecule is a sensitive function of the degree of tetrahedral symmetry present in the local molecular environment. The density-dependent variations in α_H and α_O are, however, smaller in magnitude than those of α_u reflecting their lower sensitivity to the multiple time-scale behavior of the hydrogen-bonded network. This is consistent with our earlier observations that at a given state point, crossover to white noise behavior takes place at higher frequencies in the $S_O(f)$ and $S_H(f)$ spectra then in $S_u(f)$ indicating that local tetrahedral order decorrelates faster over the hydrogen-bonded network than local configurational energy.

To summarize, the effect of increasing density and the consequent destruction of the hydrogen-bonded network in water is demonstrated in the power spectra by a loss of the distinct identity of the librational peak and by closely correlated variations in the diffusivity and the exponent of the $1/f^{\alpha}$ region. Our earlier study showed that the effect on tagged particle spectra of increasing temperature was very similar to that of increasing density in the librational and multiple time-scale regimes. However, the disorder associated with increasing thermal fluctuations had two additional effects: (i) the crossover to white noise behavior shifts to higher frequencies fairly rapidly with temperature and (ii) as thermal collisions become an important diffusional mechanism, the degree of correlation between the $1/f^{\alpha}$ exponent and the diffusivity decreases.

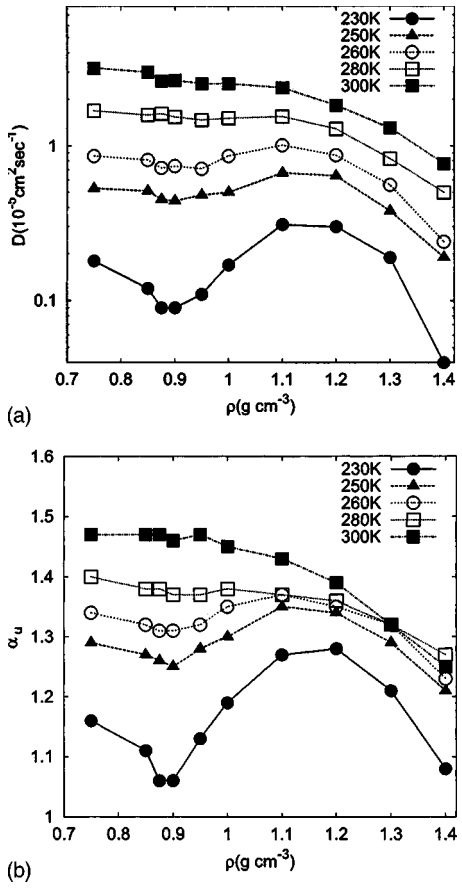

FIG. 5. Dependence on density ρ of (a) the diffusivity D and (b) the exponent α_u along isotherms at 230, 250, 260, 280, and 300 K. The exponent α_u is evaluated using the low-frequency $1/f^{\alpha}$ regime from 1 to 40 cm^{-1} at 230–280 K and over the frequency range 1–200 cm^{-1} at 300 K.

C. Defining the anomalous diffusional regime from power spectral data

The range of density over which $(\partial D/\partial \rho)_T$ is greater than zero decreases with temperature and by 300 K, the diffusional anomaly disappears. In Fig. 5, we show both diffusivity and α_u as a function of density for different isotherms in the temperature range from 230 to 340 K. It should be noted that the α_u values corespond to the low-frequency multiple time-scale regime, which has temperature-dependent frequency range. Figure 5 shows that the variations in diffusivity with density are strikingly mirrored by the corresponding isotherms for α_u. The α_{O} and α_{H} exponents show a similar correlation though the density dependence is weaker for these quantities, as pointed out in the preceding section.

Figure 6 illustrates the strong quantitative correlation $\ln D$ and α_u along the different isochores studied in this work. Only at the highest densities (e.g., 1.4 g cm^{-3}) and highest temperatures (e.g., 340 and 300 K) when the hydrogen-bond network is largely destroyed is this correlation lost. We also note that the correlation is strong even for the phase-separated states along the 0.75 g cm^{-3} isochore as well as for densities close to the spinodal density of 0.85 g cm^{-3}.

To further illustrate the connection between the diffusivity and dynamical fluctuations in the local environment, we briefly review the connection between the diffusional

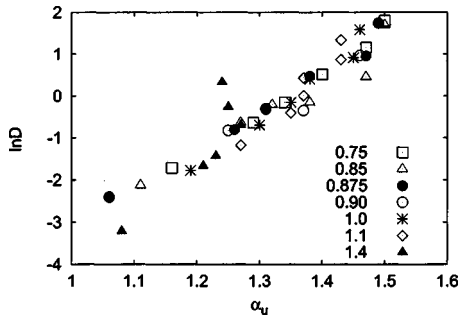

FIG. 6. Correlation plot showing $\ln D$ against α_u for different isochores. The frequency range for evaluating α_u is the same as in Fig. 5. Units of diffusivity are taken as 10^{-5} cm^2 s^{-1}.

anomaly, the density anomaly and the degree of static structural order in liquid water established in Ref. 8. In this work, a structurally anomalous region in the density-temperature plane was identified with a low density boundary defined by loci of maximum orientational order and a high-density boundary defined by loci of minimum translational order. The orientational order parameter was taken to be q_{O}. The translational order parameter τ was defined as

$$\tau = (1/\xi_c)\int_0^{\xi_c} (g(\xi) - 1)d\xi, \tag{3}$$

where $\xi = r\rho^{1/3}$ and $\xi_c = 2.83$. Within this structurally anomalous region, the translational and orientational order are strongly correlated. The region of anomalous diffusivity, defined by the loci at which $(\partial D/\partial \rho)_T = 0$, i.e., by $\rho_{\min}$ and $\rho_{\max}$, was shown to lie within this structurally anomalous region. The region of the density anomaly was shown to be nested within the region of the diffusional anomaly. It was also shown that as the degree of orientational order is increased, the structural, kinetic, and density anomalies occur in succession.

In this work, we locate the maxima and minima in the $\alpha_u(\rho)$ curves at different temperatures. Figure 7 shows the boundaries of the anomalous regimes for the structural order, the diffusivity and the density as determined from our simulation data. We also plot the loci of maxima and minima in α_u. Within the limits of statistical error associated with the

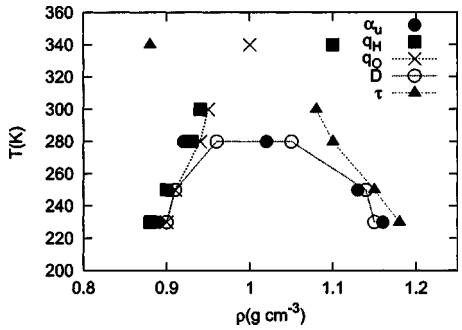

FIG. 7. Loci of maxima and minima in the diffusivity (○) and α_u (●) for temperature below 300 K. Also shown are locations of the maxima in the q_{H} and q_{O} order parameters as well as of the minima in τ. Note that state points at 340 K lie outside the region of the structural anomaly for which q_{H} reaches a plateau value and q_{O} and τ are probably not physically meaningful.

simulations and the interpolation procedure, it can be seen that the boundaries of the diffusionally anomalous regime can be determined equally well from the α_u data, as from the diffusivities.

The close connections between the diffusional anomaly and the variations in the exponent for multiple time-scale behavior demonstrated in this work suggest a possible microscopic picture for the nesting the different types of anomalous regions. Along an isotherm, as density is increased, orientational order reaches a maximum at a density ρ_q and then decreases. The onset of the diffusional anomaly occurs when orientational order is sufficiently small that translational-rotational coupling increases enough that the diffusivity begins to rise with increasing density. The high density boundary of the diffusionally anomalous region is reached when the density is suffciently high that steric or molecular size effects become large enough to dominate the density dependence of the diffusivity. Beyond this density, one can expect interparticle correlations to increase resulting in an increase in translational order. At low temperatures, the borders of the diffusionally and structurally anomalous regions will be very close, i.e., ρ_q and $\rho_{\min}$ will be very similar. As temperature increases, thermal fluctuations will provide an alternative diffusional mechanism and the correspondence between structural order and diffusivity is attenuated.

IV. CONCLUSIONS

This study establishes that the variations in mobility with pressure in the region of the diffusional anomaly are unambiguously mirrored in the exponent of the $1/f^{\alpha}$ or multiple time-scale region thus allowing one to monitor the dynamical effects of coupling the localized librational modes to the hydrogen-bonded network. The range of frequency over which $1/f^{\alpha}$ behavior is observed, including the frequency of crossover to white noise, provides a quantitative assessment of the time and length scales over which correlations in the network vanish. Moreover, multiple time-scale behavior is not equally pronounced for all observables, due to differing sensitivities to processes operating on different time scales.

The significance of the present results derive from the clear connections that can be drawn between three distinctive length and time scale features of bulk water: the local molecular environment, the hydrogen-bond network reorganizations and the diffusivity which is a long-time averaged transport property. This approach provides a possible route for understanding the connection between structural order and the static and dynamic anomalies of water and can be extended to other hydrogen-bonded systems or networked liquids.[34–36] Since power spectral analysis allows one to analyze simultaneous changes on several frequency scales and provides a signature of correlated motions in networked liquids, it provides a useful complementary approach to the analysis of time correlation functions for hydrogen-bonded systems.[37,38] In this context, it will be useful in future work to define observables which are sensitive to multiple time-scale behavior of the network and are experimentally more easily measured than local configurational energy or local order.

Our work also suggests that it would be of interest to examine the connection between $1/f^{\alpha}$ behavior and spatiotemporal heterogeneity in supercooled liquids since the distribution of length and time scales in the system is expected to widen as one approaches the kinetic glass transition. In the context of water, such a kinetic glass transition is predicted for SPC/E water around 190 K at 1 g cm^{-1};[39] the experimental value is around 225 K.[3] Near this dynamical transition, water behaves in a very similar manner to the binary Lennard-Jones glass formers with no apparent effect of the hydrogen-bond network. Our power spectral analysis shows that by 230 K, two and three-molecule vibrational modes are shifted into the Lorentzian tail, indicating that these vibrational frequencies are progressively decoupled from overall network reorganizations. As the temperature is reduced further, one would expect the multiple time-scale regime to shift to lower frequencies and involve larger clusters; the dynamics of these larger clusters may be insensitive to directional bonding and local tetrahedral order.

Our results have interesting implications for experimental work on water and aqueous solutions, specially in the context of hydration of biomolecules.[40,41] We show that different observables will have different degrees of sensitivity to the underlying multiple time-scale dynamics of the hydrogen-bonded network and therefore the choice of spectroscopic technique is likely to be significant. For example, the behavior of high-frequency librational modes as a function of density can be studied by ultrafast spectroscopy.[42] Experimental evidence for $1/f^{\alpha}$ behavior in the power spectra, or the equivalent stretched exponential behavior of time-correlation functions, exists from inelastic neutron scattering, Raman and, most recently, optical Kerr effect measurements.[43–45] The pressure or density dependence of the exponents has not been examined so far and our work indicates that these will be of considerable interest.

ACKNOWLEDGMENTS

This work was supported by the Department of Science and Technology Grant No. (SP/S1/H-16/2000). A.M. thanks CSIR, New Delhi, for the award of a Senior Research Fellowship.

[1] *Water: A Comprehensive Treatise*, edited by F. Franks (Plenum, New York, 1972).
[2] F. H. Stillinger, Adv. Chem. Phys. **31**, 1 (1974).
[3] C. A. Angell, Annu. Rev. Phys. Chem. **34**, 593 (1983).
[4] F. X. Prielmeier, E. W. Lang, R. J. Speedy, and H.-D. Lüdeman, Phys. Rev. Lett. **59**, 1128 (1987).
[5] C. A. Angell, E. D. Finch, L. A. Woolf, and P. Bach, J. Chem. Phys. **65**, 3063 (1976).
[6] H. E. Stanley, S. V. Buldyrev, N. Giovambattista *et al.*, J. Stat. Phys. **110**, 1039 (2003).
[7] P. G. Debenedetti, J. Phys.: Condens. Matter **15**, R1669 (2003).
[8] J. R. Errington and P. G. Debenedetti, Nature (London) **409**, 318 (2001).
[9] J. R. Errington, P. G. Debenedetti, and S. Torquato, Phys. Rev. Lett. **89**, 215503 (2002).
[10] O. Mishima and H. E. Stanley, Nature (London) **396**, 329 (1998).
[11] F. W. Starr, F. Sciortino, and H. E. Stanley, Phys. Rev. E **60**, 6757 (1999).
[12] P. A. Netz, F. W. Starr, M. C. Barbosa, and H. E. Stanley, Physica A **315**, 470 (2002).
[13] P. A. Netz, F. W. Starr, H. E. Stanley, and M. C. Barbosa, J. Chem. Phys. **115**, 344 (2001).
[14] A. Scala, F. W. Starr, E. La Nave, F. Sciortino, and H. E. Stanley, Nature

(London) **406**, 166 (2000).
[15]S. Harrington, P. H. Poole, F. Sciortino, and H. E. Stanley, J. Chem. Phys. **107**, 7443 (1997).
[16]F. Sciortino, A. Geiger, and H. E. Stanley, Nature (London) **354**, 218 (1991).
[17]F. Sciortino, A. Geiger, and H. E. Stanley, Phys. Rev. Lett. **65**, 3452 (1990).
[18]J. Texeira, in *Hydration Processes in Biology*, edited by M.-C. Bellissent-Funel (IOS, Amsterdam, 1999).
[19]B. Mandelbrot, *Multifractals and* $1/f$ *Noise: Wild Self-Affinity in Physics (1963-1976)* (Springer, New York, 1999).
[20]S. R. Elliot, *Physics of Amorphous Materials* (Longman Scientific and Technical, Essex, 1990).
[21]E. Milotti, Phys. Rev. E **51**, 3087 (1995).
[22]E. Milotti, $1/f$ noise: a pedagogical review. See http://lanl.arXiv.org/physics/0204033
[23]M. Sasai, I. Ohmine, and R. Ramaswamy, J. Chem. Phys. **96**, 3045 (1992).
[24]A. Mudi, R. Ramaswamy, and C. Chakravarty, Chem. Phys. Lett. **376**, 683 (2003).
[25]A. Mudi and C. Chakravarty, Mol. Phys. **102**, 681 (2004).
[26]A. Mudi and C. Chakravarty, J. Phys. Chem. **108**, 19607 (2004).
[27]A. Mudi, R. Ramaswamy, and C. Chakravarty (http://arXiv.org/abs/cond-mat/0405210).
[28]H. J. C. Berendsen, J. R. Grigera, and T. P. Straatsma, J. Phys. Chem. **91**, 6269 (1987).
[29]W. Smith and T. R. Forester, J. Mol. Graphics **14**, 136 (1996).
[30]W. Smith, C. W. Yong, and P. M. Rodger, Mol. Simul. **28**, 385 (2002). The DL_POLY website is http://www.cse.clrc.ac.uk/msi/software/DL_POLY/
[31]M. D. Allen and D. J. Tildesley, *Computer Simulation of Liquids* (Clarendon, Oxford, 1986).
[32]W. H. Press, B. P. Flannery, S. A. Teukolskyi, and W. T. Vetterling, *Numerical Recipes in FORTRAN* (Cambridge University Press, Cambridge, 1990).
[33]M. E. Parker and D. M. Heyes, J. Chem. Phys. **108**, 9039 (1998).
[34]R. M. Lynden-Bell, J. C. Rasaiah, and J. P. Noworyta, Pure Appl. Chem. **73**, 1721 (2001).
[35]D. L. Bergman and R. M. Lynden-Bell, Mol. Phys. **99**, 1011 (2001).
[36]D. Bertollini, M. Cassettrari, M. Ferrario, P. Grigolini, and G. Salvetti, Adv. Chem. Phys. **62**, 277 (1985).
[37]A. Luzar and D. Chandler, Nature (London) **379**, 55 (1996).
[38]P. Raiteri, A. Laio, and M. Parrinello, Phys. Rev. Lett. **93**, 087801 (2004).
[39]P. Gallo, F. Sciortino, P. Tartaglia, and S.-H. Chen, Phys. Rev. Lett. **76**, 2730 (1996).
[40]S. Dixit, J. Crain, W. C. K. Poon, J. L. Finney, and A. K. Soper, Nature (London) **416**, 829 (2002).
[41]*Hydration Processes in Biology*, edited by M.-C. Belissent-Funel (IOS, Amsterdam, 1999).
[42]C. J. Fecko, J. D. Eaves, J. J. Loparo, A. Tokmakoff, and P. L. Geissler, Science **301**, 1698 (2003).
[43]G. E. Walrafen, M. S. Hokmabadi, W.-H. Yang, Y.-C. Chu, and B. Monosmith, J. Phys. Chem. **93**, 2909 (1989).
[44]M.-C. Bellisent-Funel, S. Longeville, J. M. Zanotti, and S.-H. Chen, Phys. Rev. Lett. **85**, 3644 (2000).
[45]R. Torre, P. Bartolini, and R. Righini, Nature (London) **428**, 296 (2004).